Progressive Damage Modeling of Durable Bonded Joint Technology

Frank A. Leone, Carlos G. Dávila, Shih-Yung Lin, Stan Smeltzer
NASA Langley Research Center, Hampton, VA 23681

Donato Girolamo
North Carolina State University, Raleigh, NC 27695

Sayata Ghose, Juan C. Guzman, and Douglas A. McCarville
The Boeing Company, Seattle, WA 98125

ABSTRACT

The development of durable bonded joint technology for assembling composite structures for launch vehicles is being pursued for the U.S. Space Launch System. The present work is related to the development and application of progressive damage modeling techniques to bonded joint technology applicable to a wide range of sandwich structures for a Heavy Lift Launch Vehicle. The joint designs studied in this work include a conventional composite splice joint and a NASA-patented Durable Redundant Joint. Both designs involve a honeycomb sandwich with carbon/epoxy facesheets joined with adhesively bonded doublers.

Progressive damage modeling allows for the prediction of the initiation and evolution of damage. For structures that include multiple materials, the number of potential failure mechanisms that must be considered increases the complexity of the analyses. Potential failure mechanisms include fiber fracture, matrix cracking, delamination, core crushing, adhesive failure, and their interactions. The joints were modeled using Abaqus parametric finite element models, in which damage was modeled with user-written subroutines. Each ply was meshed discretely, and layers of cohesive elements were used to account for delaminations and to model the adhesive layers. Good correlation with experimental results was achieved both in terms of load-displacement history and predicted failure mechanisms.

1. INTRODUCTION

Finite element analyses were conducted to investigate the mechanical response and strength of two design concepts for joining composite sandwich panels. The first joint consists of a conventional splice joint (CSJ), and the second concept is referred to as the Durable Redundant Joint (DRJ). In this study, the strength and failure modes of both joint designs are compared to those of the pristine sandwich. All simulations account for several potential failure modes, including intralaminar damage of the carbon/epoxy facesheets and splices, compression damage in the honeycomb core, failure of the adhesive layers, and interply delaminations. The results gathered from these analyses are presented herein and compared with experimental data.

2. CONFIGURATION OF THE PANELS AND JOINTS

The sandwich panels used in this study are composed of six-ply carbon/epoxy facesheets and a 25.4-mm-thick aluminum honeycomb core, as shown in Figure 1a. The facesheet plies have a nominal thickness of 0.19 mm. The stacking sequence of the facesheets is $[+60/0/-60]_S$. The pristine panels are 559 mm long and 76.2 mm wide, with the 0° direction aligned with the specimen length.

The CSJ specimens consist of two sandwich panels joined with two 69.9-mm-long, six-ply splices bonded to the exterior faces of the sandwich with FM-300M adhesive, Figure 1b. At their thickest, the splices have the same stacking sequence as the facesheets. The splices have internal ply terminations and ply drops, and the cascading ply terminations are separated by 6.4 mm from each other. The CSJ specimens measure 559 mm long and 76.2 mm wide.

Design specifications for the joint specimens allow for a 2.54-mm gap between the sandwich panels, although it was assumed that the two sandwich panels are initially in contact. To decrease the severity of the stress concentration in the splice near the gap of a CSJ, a 12.7-mm Teflon film was inserted in-line with the adhesive layer at the joint gap.

The DRJ concept expands upon the design of the conventional splice joints by adding three hollow laminated inserts in place of honeycomb core at the joint center, Figure 1c. These inserts increase the damage tolerance of the joints by providing an additional load path within the joint. In addition, the inserts cause nearly symmetric load paths about the centerlines of the facesheets, which reduces the bending of the facesheets and the associated peel stresses. The DRJ inserts were bonded to the interior surface of the sandwich facesheets using FM-300M adhesive.

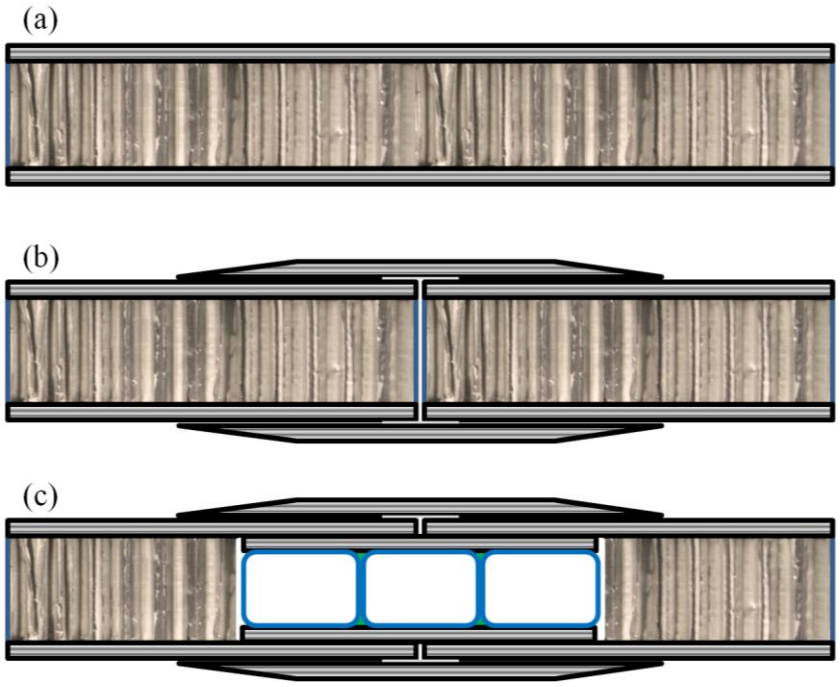

Figure 1. Schematics of the (a) pristine sandwich panel, (b) conventional splice joint, and (c) durable redundant joint.

3. PROGRESSIVE DAMAGE ANALYSIS METHODS

As with any composite structure, the sandwich panel joints considered herein have the potential to exhibit several simultaneous failure mechanisms. For example, fiber fracture and intraply matrix cracking can occur within the carbon/epoxy plies, mixed-mode delaminations are possible between the plies, the adhesive can debond, and the honeycomb sandwich core can crush. In order to account for each of these potential failure mechanisms and their many possible interactions, multiple progressive damage analysis (PDA) methodologies are required. Intraply damage is taken into account via a continuum damage mechanics (CDM) approach. Interply and adhesive damage is implemented via the inclusion of layers of cohesive elements. Honeycomb core crushing was modeled using a specialized one-dimensional damage model. The next sections briefly describe the PDA techniques used in the present analyses.

3.1 Continuum Damage Mechanics

Continuum damage mechanics is a PDA method that allows for the predictions of both damage initiation and evolution without having to make modifications to the original finite element mesh of the structure being analyzed. Rather than modeling cracks by the discrete insertion of discontinuities into the original finite element mesh, CDM approaches represent the effects of cracks by softening certain components of the constitutive stiffness tensor. Different damage modes are accounted for with a set of scalar damage state variables. After the initiation of damage, the affected stiffness terms are softened according to relevant fracture toughness properties and the local characteristic element size. As a result, in order to accurately predict the initial linear elastic response, the initiation of damage, and the evolution of damage, it is necessary to have a set of material property data including the elastic moduli, strengths and fracture toughness values for each potential failure mechanism.

A combination of the LaRC03 [1] and LaRC04 [2] failure criteria were used for the CDM model predictions. The LaRC set of criteria consists of stress-based analytical equations that predict the onset of failure mechanisms such as matrix cracking, fiber fracture, and fiber kinking. The prediction of damage evolution was implemented through an updated version of the CDM approach originally proposed by Maimí et al. [3]. The improvements to the CDM approach that are relevant to this work include: (1) an extension of the set of failure criteria to account for three-dimensional stress states, as well as extensions to the corresponding damage evolution laws and stiffness tensor degradation algorithms; (2) the development of a mixed-mode matrix damage evolution law [4]; and (3) the development of a new definition for the CDM effective stresses that allow for the simultaneous evolution of multiple damage modes.

3.2 Cohesive Zone Modeling

Layers of zero-thickness cohesive elements were used between all plies of different orientations to account for the potential of delaminations developing. Cohesive elements are specialized nonlinear finite elements that are particularly useful to predict the initiation and evolution of cracks when the potential propagation paths are known a priori, e.g., Turon et al. [5].

The constitutive response of cohesive elements is defined using a cohesive law, defined in terms of local traction versus crack opening displacement. Prior to the prediction of damage initiation, a high cohesive stiffness keeps the crack surfaces closed. Upon satisfying a failure criterion, the stiffness properties of the element soften with further deformation until the element completely

fails. The crack opening displacements corresponding to damage initiation and complete failure are dependent on the mode I and mode II strengths and fracture toughness values, as well as the local mode mixity. No in-plane loads are carried by cohesive elements.

In the present work, cohesive elements are also used in a novel approach to represent the response and failure of the adhesive layer. When used in this mode, the cohesive elements have the true thickness and the compliance of the adhesive layer.

3.3 Core Crush Model

To represent the loss of stiffness of a honeycomb core as a result of crushing under compressive normal loads, a custom one-dimensional damage model is used [6]. This damage model separates the compressive normal response of a honeycomb material into three parts: (1) the initial linear-elastic response, characterized by the Young's modulus; (2) the crushing of the core, during which the material has a negative tangent stiffness; and (3) post-crushed response, characterized by a significantly reduced modulus. In addition, the core crush damage model is capable of representing the unloading/reloading response of either a partially or fully crushed material.

This damage model is one-dimensional—it represents only the response of the normal direction of the core. Therefore, this model does not represent the transverse shear response of the honeycomb core.

4. MATERIAL PROPERTIES

As for any analysis, the reliability of predictions obtained with progressive damage analyses can only be as good as the quality of the input material properties. While the errors in the predictions of failure in linear analyses are likely to be of a magnitude comparable to the uncertainty in the input strength data, the errors in PDA models can exhibit a much greater sensitivity to incorrect material properties, especially for structures that exhibit multiple damage modes and damage evolution before structural failure. As a result, it is strongly recommended to use reliable material strength and fracture toughness properties for PDA models when available, and, to independently characterize the materials of interest when possible. Unfortunately, PDA models require material data that is often not available, and cost and scheduling constraints prevent the undertaking of a complete material characterization. Such is the case for the present effort. The material properties used herein were assembled from several sources, and, for those properties that were not available, the corresponding properties of a similar material were used.

4.1 Carbon/Epoxy Plies (TE-1, Grade 190, Type 35, Prepreg Tape)

The material properties used for the carbon/epoxy plies in the facesheets and doublers are shown in Table 1. The elastic, thermal, and strength properties were provided by The Boeing Company. The mode I and mode II matrix fracture toughness properties, G_{YT} and G_{SL}, and Benzeggagh-Kenane mixed-mode factor η, are those of IM7/977-2, published by Reeder [7]. These properties were used for the prediction of both intraply matrix cracking and interply delaminations. The availability of fiber fracture toughness properties, G_{XT} and G_{XC}, is extremely limited in the literature. As a result, the well-documented fiber fracture toughness properties of IM7/8552, another toughened epoxy system of similar performance, were used in this investigation.

Table 1. TE-1 Grade 190 Type 35 Carbon/Epoxy tape Material Properties.

Elastic Properties		
E_{11}	142.0	GPa
E_{22}	7.8	GPa
E_{33}	7.8	GPa
G_{12}	4.0	GPa
G_{13}	4.0	GPa
G_{23}	2.8	GPa
ν_{12}	0.34	
ν_{13}	0.34	
ν_{23}	0.40	

Strength Properties		
X_T	2606.	MPa
f_{XT}^{*}	0.069	
X_C	−1682.	MPa
f_{XC}^{*}	0.069	
Y_T	72.4	MPa
Y_C	−299.	MPa
S_L	116.	MPa
$S_T^{\dagger}$	112.	MPa

Fracture Properties		
G_{XT}^{*}	146.7	N/mm
f_{GXT}^{*}	0.822	
G_{XC}^{*}	106.3	N/mm
f_{GXC}^{*}	0.822	
$G_{YT}^{\ddagger}$	0.26	N/mm
$G_{YC}^{\dagger}$	2.33	N/mm
$G_{SL}^{\ddagger}$	1.40	N/mm
$\eta^{\ddagger}$	1.4	

Thermal Properties		
α_{11}	1.11e−8	/°C
α_{22}	1.00e−5	/°C
α_{33}	1.00e−5	/°C

* IM7/8552 properties [8, 9].
† Calculated
‡ IM7/977-2 properties [7].

4.2 FM-300M Adhesive

Prior to this study, there was no satisfactory source for the strength and fracture properties for the adhesive used in this program at its implemented thickness. Due to the importance of these material properties, a thorough characterization study was conducted by Girolamo [10].

Girolamo used three characterization specimen types to determine the mode I, mode II, and mixed-mode fracture properties. Digital image correlation (DIC) was used to extract the displacement histories around the specimen crack tips. The displacement data was processed to extract the history of the shearing and opening displacement jumps across the crack tips. Following an inverse methodology, these displacement jumps were then substituted into analytical J-integral equations that describe the fracture energy. Finally, the cohesive laws were obtained by numerical derivation of the J-integral functions. The resulting cohesive laws represent the adhesive stiffness, its strength, and its fracture resistance in the form of stress-displacement functions in each mode of fracture.

The measured cohesive laws were approximated using piecewise linear functions for numerical implementation, and using two superposed cohesive elements to represent the nonlinear response. The material properties used in the modeling of the joint specimens are listed in Table 2.

Table 2. FM-300M Material Properties.

Elastic Properties		
$K_{I\text{-}A}$	23823	N/mm^3
$K_{II\text{-}A}$	2000	N/mm^3
K_{I_B}	444	N/mm^3
$K_{II\text{-}B}$	200	N/mm^3

Strength Properties		
$\sigma_{I\text{-}A}$	71.	MPa
$\sigma_{II\text{-}A}$	46.	MPa
$\sigma_{I\text{-}B}$	9.	MPa
$\sigma_{II\text{-}B}$	22.	MPa

Fracture Properties		
$G_{Ic\text{-}A}$	0.70	N/mm
$G_{IIc\text{-}A}$	3.50	N/mm
$G_{Ic\text{-}B}$	0.55	N/mm
$G_{IIc\text{-}B}$	7.79	N/mm
η_A	2.6	
η_B	2.2	

4.3 Honeycomb Core

The aluminum honeycomb material used in the bonded joint specimens is Hexcel CR III 1/8-5052-.0007. The compression normal modulus and strength of the honeycomb material are 517 MPa and 2 MPa, respectively, according to the manufacturer. As mentioned, the honeycomb damage model elements used were not capable of representing the transverse shear response of the core, so no additional properties were required to define the initial linear-elastic response.

Several of the stresses and strains required by the honeycomb material damage model were not available. As a result, assumptions were made regarding the behavior of the honeycomb material after the initiation of the crushing failure mechanism. By analogy with other aluminum honeycomb cores, it was assumed that after exceeding its compressive strength, the core would crush and the reaction load would drop by half at −0.8% deformation. Further compression of the core would cause the load to increase gradually with a tangent stiffness equal to one percent of the initial stiffness. It was found that the predicted results were relatively insensitive to the material properties related to the post-crush response.

5. FINITE ELEMENT MODELS OF BONDED COMPOSITE JOINTS

The PDA finite element models of the joint specimens were solved using Abaqus 6.10-1. Custom user subroutines were used to define the constitutive responses of carbon/epoxy plies (via CDM) and the honeycomb core material. Due to the convergence difficulties associated with softening materials, the models were solved with Abaqus/Explicit. Elements were not removed from consideration after failing for either the CDM or cohesive damage methods.

The models were solved in two steps: the first one takes into account residual thermal stresses from the joint curing process, and a second consists of the load application. For computational efficiency, the time periods of the steps were selected to be as short as possible without inducing any significant dynamic forces. Time periods of 0.005 and 0.05 second were used for the thermal and load application steps, respectively. Loading rates were increased sinusoidally to reduce any accelerations applied to the models. Variable mass scaling was used to decrease the solution time by increasing the minimum stable time increment to 2.e−07 second throughout the models (i.e., ensuring that less than the recommended limit of 2.e+06 increments were used). Mass scaling factors were updated every 500 solution increments to account for any local changes in element stiffness.

5.1 Pristine Sandwich Panel

The pristine panel represents the composite component whose response and strength is used as a reference for comparison with the joint models. Because the pristine panel is devoid of stress concentrations, it is not necessary to model the full length of the pristine panel. Instead, a model of reduced dimensions was created. The model of the pristine panel specimen represents a panel that is 25.4 mm long and 6.4 mm wide, as shown in Figure 2a. Symmetry is assumed through the center of the honeycomb core. The short edges of the model are constrained in the facesheet planar directions, with the long edges left free. In order to avoid premature failure near the boundary conditions, 3.2 mm of material from both constrained edges is modeled with elements with a linear-elastic constitutive response. Loads were applied uniformly by displacing one of the short model edges.

Each ply of the facesheet is represented with a single layer of solid three-dimensional (3D) reduced integration elements, C3D8R. Between each ply, a layer of zero-thickness COH3D8 cohesive elements is included. The approximate in-plane element size (i.e., edge length) for the solid and cohesive elements is 0.38 mm. The in-plane size of the honeycomb core mesh was selected to coincide with the core cell size. The much coarser mesh of the honeycomb core is connected to the underside of the facesheet mesh using tie constraints.

5.2 Conventional Splice Joint (CSJ)

The parametric conventional splice joint model expands upon the model of the pristine sandwich model by adding a six-ply doubler to join two identical pristine panels. The model is defined parametrically so that the length of the splice, the length/presence of a Teflon insert, the thicknesses of the plies and the adhesive, the locations of the ply terminations, the length of the ply drops, and mesh densities throughout the model can be adjusted to incorporate minor design changes. Each ply in the facesheets and splices is represented with a single layer of 3D solid elements through-the-thickness. The in-plane element size is equal to the ply thickness. Layers of zero-thickness cohesive elements are located between all plies of different orientations. The honeycomb core is represented by a layer of two-node T3D2 truss elements, oriented vertically.

The layer of adhesive between the facesheets and the splices is modeled using two coincident layers of finite-thickness, bilinear COH3D8 cohesive elements. The Teflon insert near the joint gap is represented by setting the strength and fracture toughness properties of the adhesive elements to extremely low values, causing them to fail very early in the analyses. As such, the elements representing the Teflon can carry compressive loads, but no shear or tensile loads.

Two planes of symmetry are assumed: at the joint center, and through the center of the honeycomb core. In addition, only 101.6 mm along the length of the quarter specimen are modeled, assuming that a relatively uniform strain state is present away from the end of the splice. For the tensile loading cases studied herein, symmetry boundary conditions are applied along the splice plies at the joint center, leaving the facesheet nodes free. Loads are applied by uniformly displacing the right side of the facesheet and honeycomb core. To reduce the analysis times, the CSJ models were solved with a highly reduced width of 1.52 mm (i.e., 8 elements).

5.3 Durable Redundant Joint (DRJ)

The DRJ model expands further on the parametric definition of the CSJ model. The honeycomb sandwich and exterior doublers of the DRJ and CSJ specimens are identical, and, as a result, only the removal of the inner 50.8 mm of the honeycomb core truss elements from the CSJ model is required to accommodate the additional DRJ inserts.

Due to the larger number of plies in the joint area relative to the pristine sandwich facesheets, it was assumed that no significant damage would develop in the DRJ inserts. The inserts are represented with S4R shell elements with linear elastic stiffness properties and are not capable of modeling damage. The layer of adhesive connecting the DRJ inserts to the interior surface of the facesheets is modeled with two layers of coincident bilinear cohesive elements. The shell elements representing the DRJ inserts are tied to the bottom surface of the cohesive elements that represent the adhesive.

Symmetry boundary conditions are applied along the splice plies and the DRJ inserts at the joint center, leaving the facesheet nodes free. As in the CSJ model, symmetry was also assumed along

the center lines of the honeycomb core and the DRJ inserts. In order to reduce the analysis times, the DRJ models were solved with a reduced width of 2.48 mm (i.e., 13 elements), thicker than the CSJ model due to the larger total thickness of the facesheet and two doublers in the DRJ. Loads were applied by uniformly displacing the right side of the facesheet and honeycomb core.

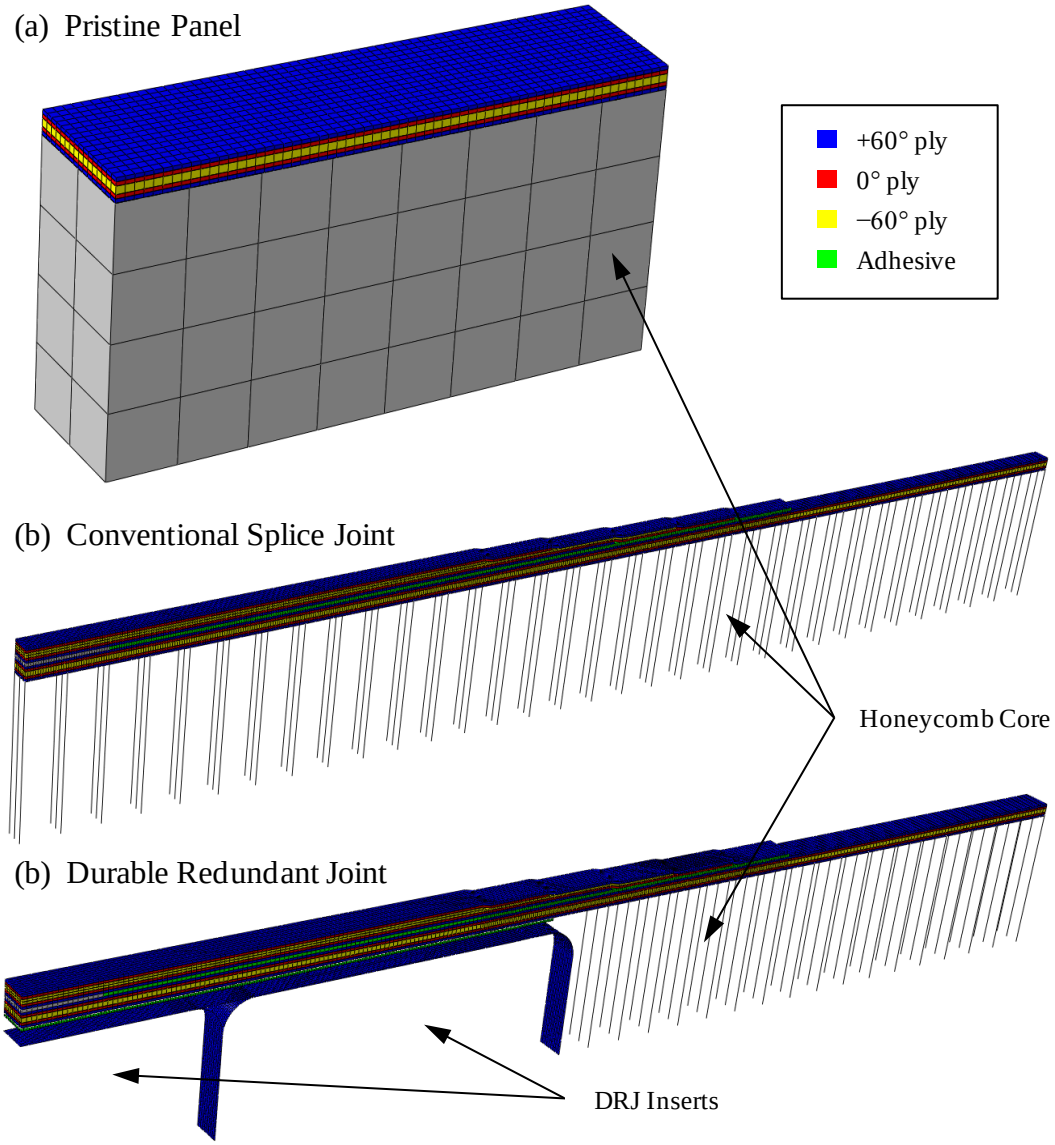

Figure 2. FE meshes for the (a) pristine sandwich panel, (b) conventional splice joint, and (c) durable redundant joint.

6. RESULTS OF BONDED COMPOSITE JOINT MODELS

6.1 Strength Predictions and Failure Mechanisms

For each of the specimens and loading cases that were analyzed, comparisons were made to the experimental results in terms of overall structural load-displacement and the manner in which

damage evolves. For each of the experiments, load-displacement results were recorded. Damage was characterized experimentally by high-resolution digital cameras and DIC systems monitoring the top, bottom, and/or cross-sections of the specimens. Because of the unpredictability of the exact location and timing of damage initiation and evolution in experiments, direct comparisons between the experimental and computational results are limited.

Due to the reduced dimensions of the models, it was necessary to scale-up the loads and displacements for comparison with the experimental results. The loads in the models were increased by scale factors equal to the ratio of the width of the full specimen to the width of the model and accounting for the quarter symmetry of the models. To obtain model displacements that can be compared to the experimental applied displacements, it was necessary to take into account the displacement along the length of the specimen that was not modeled. This additional displacement is a function of the reaction load, the length not included in the model, the undamaged laminate stiffness, and the cross-sectional area of the laminate.

6.1.1 Pristine Sandwich Panel

The analysis indicates that damage in the pristine sandwich panels starts at an applied load of approximately 62 kN in the +60° plies. At 101 kN, matrix cracking initiates in the two interior −60° plies. These cracks cause the subtle load drop visible in the load-displacement plot shown in Figure 3a. After this point, widespread matrix cracking accumulates throughout the +60° and −60° plies until the predicted panel strength, which is 158 kN. It can be observed that the strength of the specimen is approximately equal to the strength of the four 0° plies.

Both of the pristine panel specimens that were tested failed in the vicinity of the load grips, indicating that the pressure applied at the grips may have introduced unintentional stress concentrations, causing premature failure. As a result, there is no experimental data available for a direct comparison with failure load predictions. However, a good correlation between the experimental and computational in-plane stiffness was obtained.

6.1.2 Conventional Splice Joint

Excellent correlation was observed between the experimental and computational results for the conventional splice joints in terms of load-displacements results as well as the sequence of failures leading to ultimate specimen fracture. The predicted load-displacement curve for the CSJ tension specimen is shown in Figure 3b. The predicted peak load of the CSJ specimen is approximately 125 kN, compared to the experimentally observed strengths of 109 and 113 kN.

Prior to the predicted failure of the joint specimen, several instances of localized damage development occur in the model. At approximately 15 kN applied load, prior to the prediction of any intraply or interply cracks, the adhesive layer begins to soften immediately ahead of the Teflon insert. The softening of the adhesive is a very gradual process, as expected due to the relatively large fracture toughness values determined during the material characterization work. As a result, no significant load redistribution occurs due to the initial softening of the adhesive, as is indicated in Figure 3b.

Localized matrix cracking is predicted to occur at two “hot spots” in the CSJ model between 40 and 45 kN applied load: in the top 60° ply of the facesheet near the termination of the last 0° splice ply, and in the bottom 60° ply of the splice near the end of the Teflon insert. These cracks initially have no effect on the global load-displacement response.

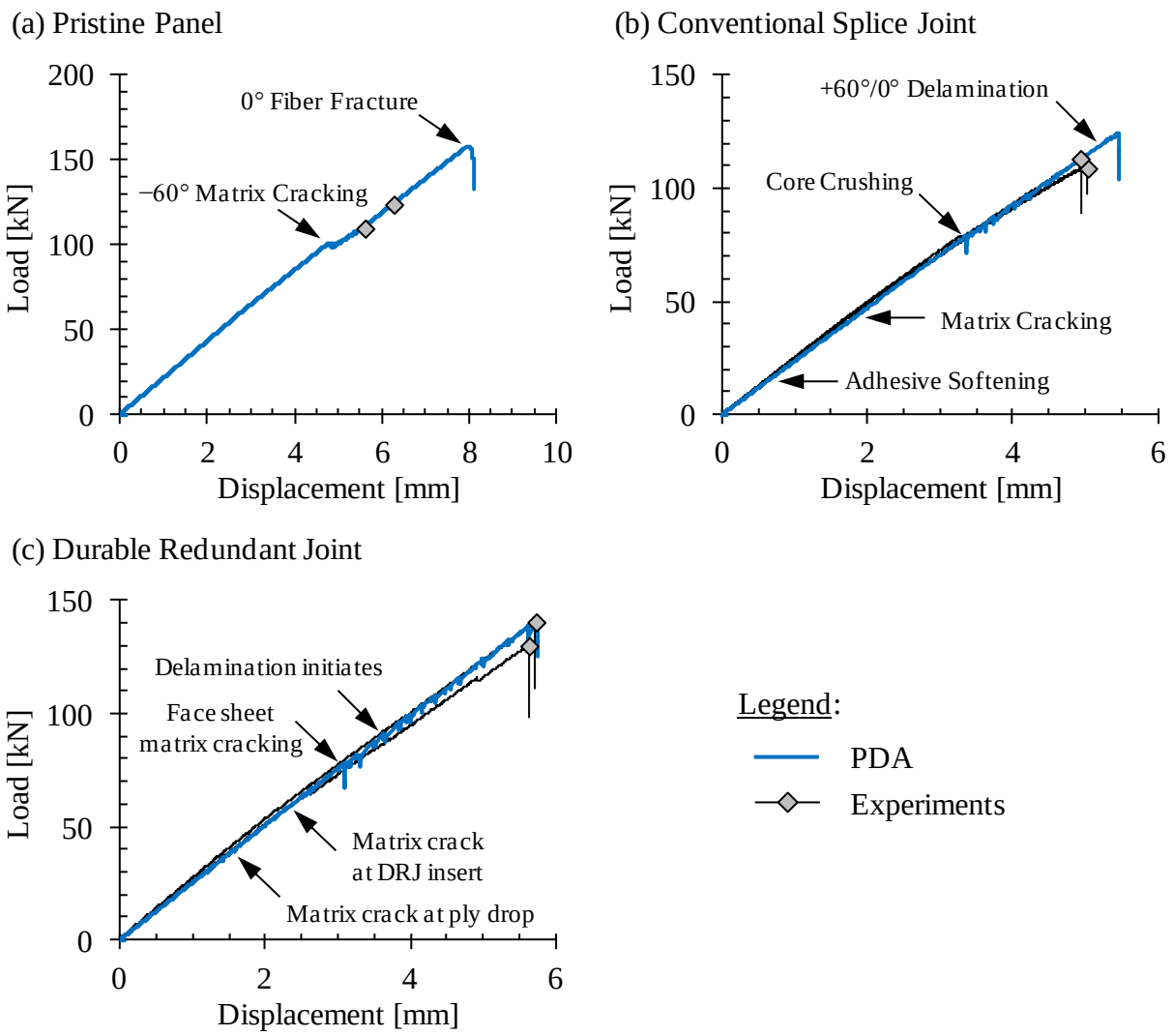

Figure 3. Load-displacement plots of the (a) pristine panel, (b) CSJ, and (c) DRJ.

The eccentricity in the load path due to the splices causes bending of the facesheet near the end of the Teflon insert, causing compressive loads in the honeycomb core in excess of its strength. At an applied load of 78 kN, the core fails by buckling of the walls of the two rows of cells closest to the joint center (i.e., four in total, assuming symmetric damage), as shown in Figure 4a. This core crush mechanism was observed experimentally, as shown in Figure 5. Widespread matrix cracking is predicted in the facesheet at 79 kN, causing a noticeable drop in the load-displacement response. At 123 kN, delaminations develop between the 60° and 0° plies at the locations of the first two 60° matrix cracks, as shown in Figure 4b. The delaminations at both locations are approximately 1.3 mm long at this load level. The delamination originating near the Teflon insert continues to grow to a length of 3.8 mm, when the peak load of 125 kN is reached, Figure 4c. Unstable delamination propagation ensues, eventually linking up with the delamination near the Teflon insert, cracking the matrix and adhesive where they meet.

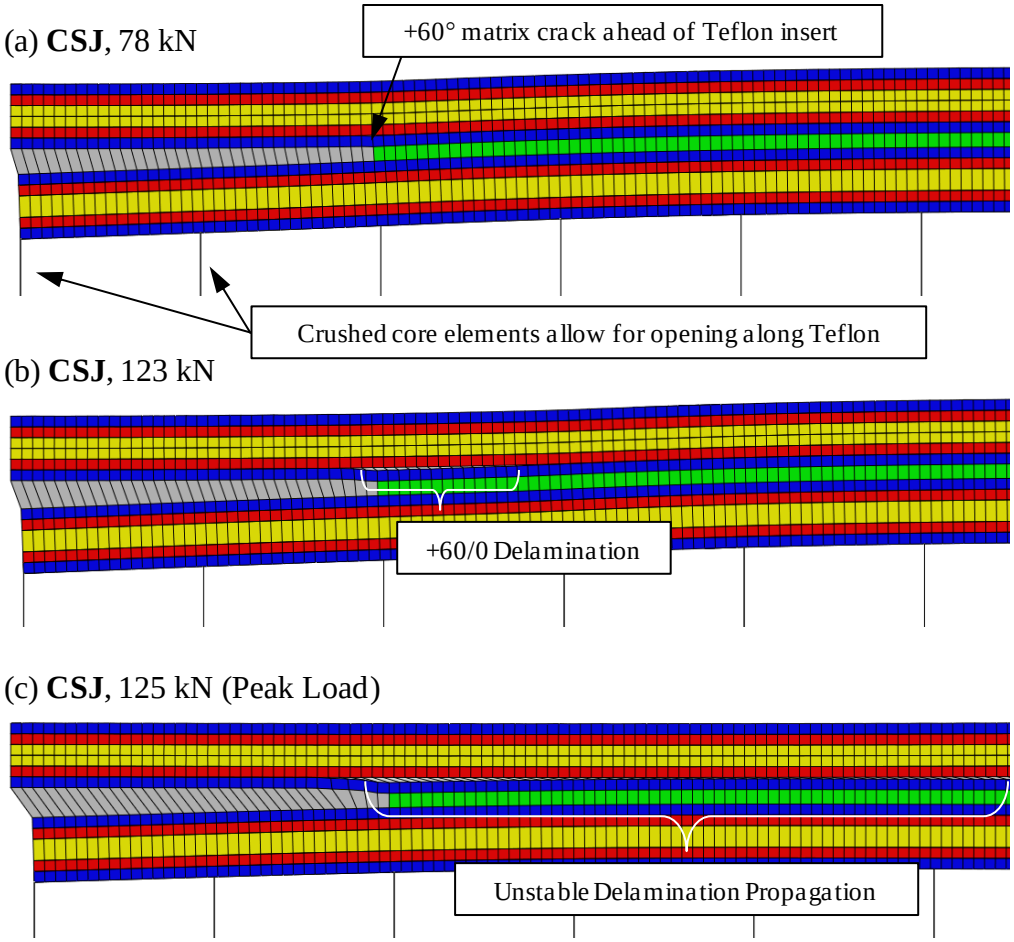

Figure 4. Failure process for conventional splice joint.

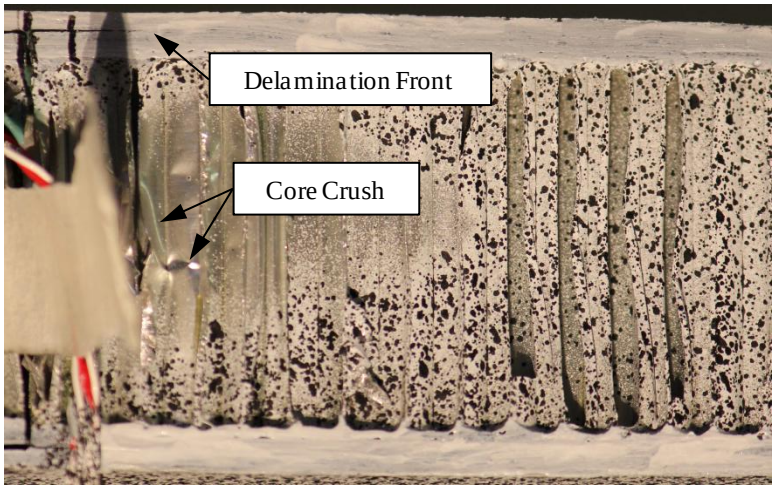

Figure 5. Digital photograph of a CSJ. The crushed core and the separation of the facesheet and splice along the Teflon insert are clearly visible.

6.1.3 Durable Redundant Joint

While the predicted sequence of damage mechanisms is very similar between the CSJ and DRJ models, the inclusion of the DRJ inserts in the joint design moves the significant damage developments outside the reinforced region of the joint, as can be seen in Figure 6. In fact, no matrix cracks or adhesive damage is predicted in the doubly reinforced region prior to the predicted joint failure.

Matrix cracks form early at two locations in the facesheet: in the top 60° ply of the facesheet near the termination of the last 0° splice ply, and in the bottom 60° ply of the facesheet just outside the DRJ inserts. These two cracks occur at 40 and 61 kN, respectively, Figure 3c. Softening of the adhesive layers between the splice and the facesheet and between the facesheet and the inserts starts at very low loads, but does not grow to a significant length before matrix cracking initiates. Widespread matrix cracking in the unbounded section of the facesheet occurs later, at 77 kN applied load.

A delamination between the 60° and 0° plies of the facesheet near the ply terminations forms at 90 kN applied load, Figure 7a. At this time, the region of softened adhesive extends approximately 1.0 mm from the termination of the 0° splice ply and 0.8 mm from the insert edge. This delamination propagates toward the joint center until reaching an approximate length of 1.5 mm at the peak load of 139 kN, Figure 3c. At this point, the two softened adhesive regions extend 3.3 mm from the 0° ply termination and 24.1 mm from the insert edge, Figure 7b.

After reaching the peak load, damage propagates inward toward the Teflon insert (i.e., to the left in Figure 7c) from both the insert/facesheet interface and the ply termination delamination. These two damage fronts are each predicted to link up with the Teflon insert, completely separating the facesheet from the inner and outer splices. Cracks originating at these two locations were observed experimentally, Figure 6.

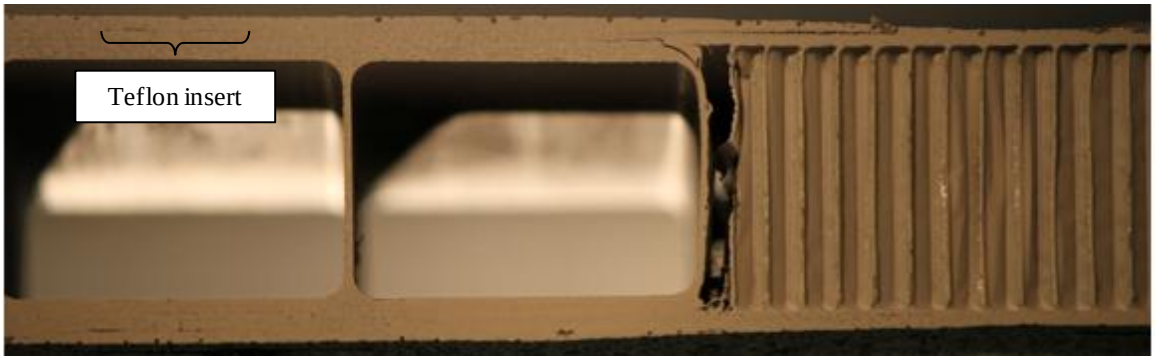

Figure 6. Digital photograph of cross-section of a DRJ specimen, just prior to failure.

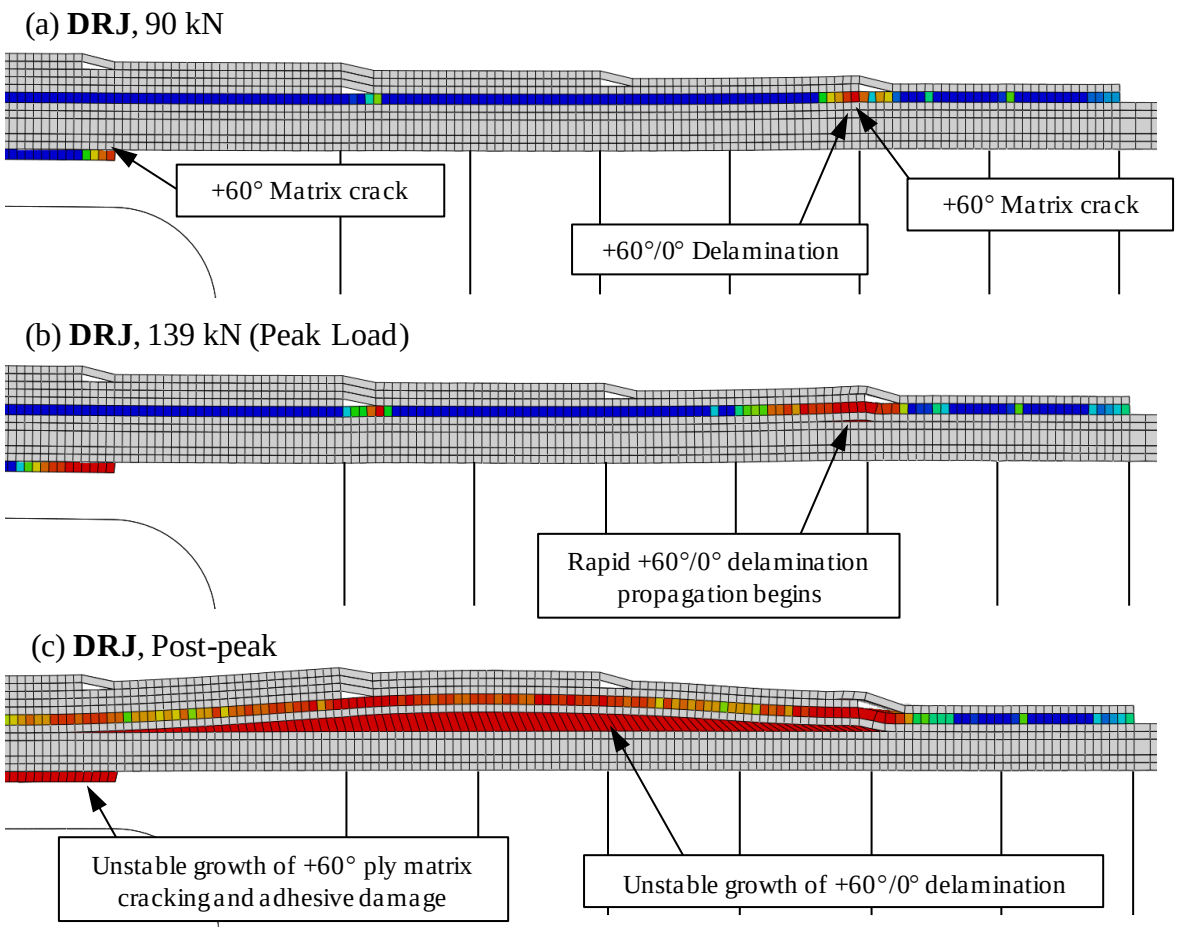

Figure 7. Failure process for the DRJ. The adhesive and interply delamination damage variable is shown in the subplots, with blue representing intact material and red representing damage.

6.2 Effect of the Teflon Insert Length on the Conventional Splice Joint Strength

A computational study was conducted on the effect of the length of the Teflon insert in the CSJ models on the predicted strength and failure mechanisms when subjected to tensile loading. The length of the Teflon insert in the CSJ model was increased in 6.4-mm increments from 0.0 to 25.4 mm. The parametric formulation of the finite element models required changing of only a single value in the model input. All other material properties and geometries were kept constant. The load-displacement results of this study are shown in Figure 8.

For the models without an insert and with a shorter 6.4-mm insert, the predicted failure mechanism remained unchanged from the 12.7-mm case: unstable +60°/0° delamination propagation from the center of the joint proceeded by matrix cracking and core crushing. However, shorter Teflon inserts cause less severe stress states in the adhesive, and, accordingly, less softening of the adhesive early in the simulation. When the adhesive layer softens, it diminishes the severity of the interply stress concentration in the splice by transferring the load from the facesheet to the splice over a longer region, delaying the onset of matrix cracking and interply delamination. This leads to the delaminations forming and propagating at lower applied loads of 114 and 117 kN, respectively.

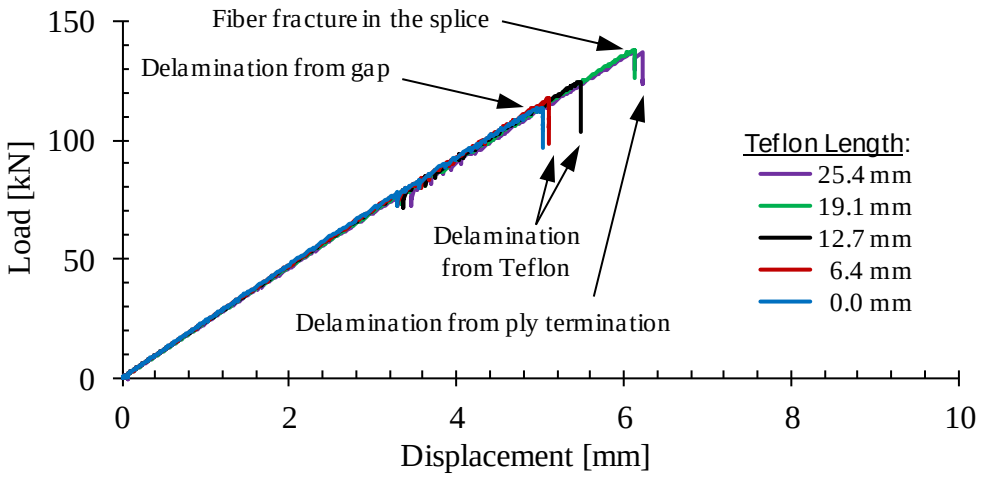

Figure 8. The predicted peak loads of the CSJ models for various Teflon insert lengths.

While the peak +60°/0° interply loads in the splice decrease as the failure process zone of the adhesive grows, another stress concentration in the bottom 0° ply of the splice is unaffected by the adhesive softening. This stress concentration is related to the bending of the splice in the vicinity of the Teflon insert due to the eccentricity of the load path through the joint. The crushing of the core beneath the insert causes additional bending, which further increases the fiber stresses of 0° ply. For the 19.1-mm insert, fiber fracture is predicted in the 0° splice plies at this location at 138 kN applied load. Because this failure mechanism is independent of adhesive softening, further increases in the insert length do not improve joint performance, as confirmed by the 25.4-mm insert case. The 25.4-mm insert model fails at a peak load of 138 kN via +60°/0° delamination originating near the outer 0° ply termination in the facesheet (i.e., the predicted DRJ failure mechanism).

7. CLOSING REMARKS

Progressive damage finite element analyses were conducted for two composite sandwich adhesively bonded joint designs to predict the load-displacement response and failure mechanism(s) and to compare the results with experimental results. The two joint designs evaluated consist of a conventional composite splice joint (CSJ) and a new NASA-patented Durable Redundant Joint (DRJ) design. A series of experiments were conducted to determine strength and failure mechanism for each joint design.

The nonlinear finite element analyses are capable of representing the initiation and evolution of several damage modes, including intraply fiber fracture, matrix cracking, interply delamination, adhesive failure, honeycomb core crushing, and their interactions. All of the models used in the analyses of the joints are three-dimensional. However, the width and length considered by the models was reduced for computational efficiency. After optimization of the explicit analysis parameters, such as loading speed and mass scaling, analysis times of 2 to 8 hours were achieved on a desktop computer. All models were written parametrically to ensure that the model configuration, material properties, boundary conditions, etc. could be easily modified.

Excellent correlation was established between the experimental and computational results for the joint specimens. Both specimens were predicted to exhibit a complex sequence of interacting

failures, involving intraply matrix cracking, core crushing, adhesive softening, and interply delaminations. Though only limited experimental data is available, studying the post-mortem photographs of the failed specimens indicates that the correct failure planes were predicted. The predicted failure loads for the CSJ and DRJ were within 13% of the experimental values.

One of the major driving forces behind the development and application of new progressive damage analysis methods is the potential reduction of the experimental testing required to validate and optimize new structures and systems. By developing a sufficiently fine model and validating it for a few bounding cases, several intermediate values of design parameters can be evaluated quickly and cheaply. An example of the application of damage models for design optimization is performed, in which the parametric CSJ model is used to evaluate the sensitivity of the joint failure loads and failure mechanisms to the dimensions of a Teflon insert. With small variations of the length of this insert, three different critical failure mechanisms were observed, and an approximate 20% improvement in the peak load of the joint was predicted.

8. REFERENCES

1 Dávila, C. G. & Camanho, P. P. "Failure Criteria for FRP Laminates in Plane Stress." NASA/TM-2003-212663.

2 Pinho, S. T., Dávila, C. G., Camanho, P. P., Iannucci, L. & Robinson, P. "Failure Models and Criteria for FRP Under In-Plane or Three-Dimensional Stress States Including Shear Nonlinearity." NASA/TM-2005-213530.

3 Maimí, P., Camanho, P. P., Mayugo, J.-A. & Dávila, C. G. "A Thermodynamically Consistent Damage Model for Advanced Composites." NASA/TM-2006-214282.

4 Leone, F. A. & Dávila, C. G. "Mixed-Mode Matrix Damage Evolution in Continuum Damage Mechanics." *16th International Conference on Composite Structures*. Porto, Portugal, 23–30 June 2011.

5 Turon, A., Camanho, P. P., Costa, J. & Dávila, C. G. "A damage model for the simulation of delamination in advanced composites under variable-mode loading." *Mechanics of Materials* 38 (2006): 1072–1089.

6 Ratcliffe, J. G., Czabaj, M. W. & Jackson, W. C. "A Model for Simulating the Response of Aluminum Honeycomb Structure to Transverse Loading." *2012 American Society for Composites 27th Technical Conference*; *15th US-Japan Conference on Composite Materials Meeting*. Arlington, VA, 1–3 October 2012.

7 Reeder, J. R. "3D Mixed-Mode Delamination Fracture Criteria–An Experimentalist's Perspective." *21st Annual Technical Conference of the American Society for Composites*. Dearborn, MI, 17–20 September 2006.

8 Camanho, P. P., Maimí, P. & Dávila, C. G. "Prediction of size effects in notched laminates using continuum damage mechanics." *Composites Science and Technology* 67 (2007): 2715–2727.

9 Catalanotti, G., Camanho, P. P., Xavier, J., Dávila, C. G. & Marques, A. T. "Measurement of resistance curves in the longitudinal failure of composites using digital image correlation." *Composites Science and Technology* 70 (2010): 1986–1993.

10 Girolamo, D. "Progressive Damage Analysis of Bonded Composite Joints." (Master's Thesis). TU Delft. 2012.